



Single crystal growth and characterization of nearly stoichiometric LiVO_2

W. Tian^{a,b,*}, M.F. Chisholm^b, P.G. Khalifah^b, R. Jin^b, B.C. Sales^b,
S.E. Nagler^b, D. Mandrus^{a,b}

^aDepartment of Physics and Astronomy, The University of Tennessee, Knoxville, TN 37996, USA

^bCondensed Matter Sciences Division, Oak Ridge National Laboratory, Oak Ridge, TN 37831, USA

Received 18 February 2004; received in revised form 18 February 2004; accepted 27 March 2004

Abstract

LiVO_2 undergoes an imperfectly understood orbital ordering transition near 500 K resulting in a loss of magnetic moment below the transition. Studies of the transition have been hampered by a lack of high-quality stoichiometric single crystals. Here we report the growth and basic characterization of large, nearly stoichiometric LiVO_2 single crystals. The crystals were characterized by magnetic susceptibility, electrical resistivity, differential scanning calorimetry, and specific heat measurements over a temperature range from 2 to 650 K. A first-order phase transition with large hysteresis near $T_t \approx 500$ K was observed in all measurements. An anisotropy of the order of 100 was observed in the in-plane versus out-of-plane resistivity, and the inferred semiconducting energy gap was 0.18 eV for $T < T_t$ and 0.14 eV for $T > T_t$. Electron diffraction experiments were performed on LiVO_2 single crystals at temperatures below and above T_t . Superlattice reflections were observed below T_t and disappeared upon heating above the phase transition temperature. Upon cooling below T_t , the superlattice spots reappeared. Bright field electron micrographs indicate that the crystals develop a roughly hexagonal network of cracks.

© 2004 Elsevier Ltd. All rights reserved.

Keywords: A. Oxides; B. Crystal growth; C. Electron diffraction; D. Magnetic properties

1. Introduction

The layered oxides LiMO_2 ($M = \text{Co}, \text{V}, \text{Ni}$) have been studied extensively for possible use as insertion electrodes in rechargeable lithium batteries [1–4]. They also show interesting structural and magnetic behavior involving the frustration present in these systems. LiVO_2 is of particular interest

* Corresponding author. Tel.: +1-865-5763985; fax: +1-865-5744814.

E-mail address: wtian@utk.edu (W. Tian).

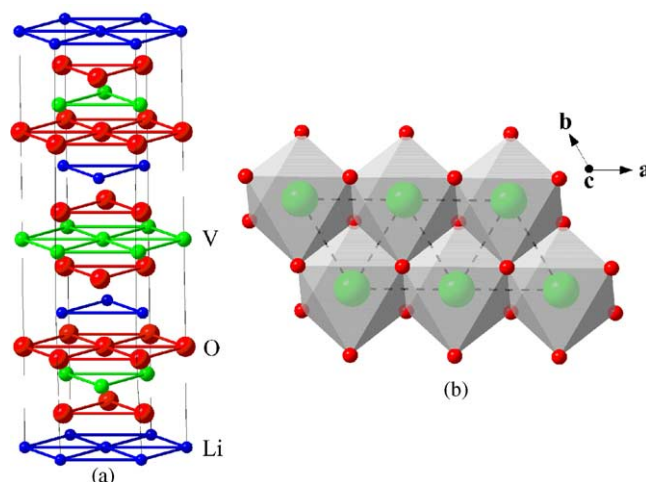
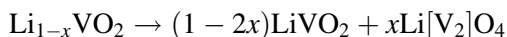


Fig. 1. Crystal structure of LiVO_2 . Part (a) is drawn to emphasize the layered quasi-2D nature of the material. Part (b) is drawn to emphasize the coordination polyhedra and the triangular sublattice of V ions.

because of its exotic ground state. Magnetic V^{3+} ($S = 1$) ions in this compound form a two-dimensional triangular lattice [5–9]. LiVO_2 was first reported by Bongers [5] to undergo a first-order magnetic transition at about $T_t = 500$ K, the system changing from a high-temperature paramagnetic phase with Curie–Weiss susceptibility to a low-temperature nonmagnetic phase without any sign of long-range magnetic order [10]. Goodenough [7,10] suggested the formation of triangular vanadium clusters (“trimers”) in the low-temperature region as a possible mechanism for this unusual phase transition. In this model the exchange coupling between the spins within the cluster is much larger than between spins in neighboring clusters, and a spin-singlet ground state is realized [11]. Recently, based on the “trimer” conjecture, a theoretical calculation suggests that this phase transition is driven by a peculiar type of orbital ordering that removes the frustration inherent in the triangular lattice and favors singlet formation [12].

LiVO_2 crystallizes in a rhombohedral structure, space group $R\bar{3}m$, with hexagonal lattice constants $a = 2.83$ Å and $c = 14.87$ Å [11]. As illustrated in Fig. 1a, Li, V and O ions occupy alternating (1 1 1) cubic planes and stack along the c -axis direction. Each of these planes forms a triangular two-dimensional lattice. Fig. 1b shows that VO_6 octahedra of trigonal symmetry share their edges to form a triangular V lattice. As the vanadium planes are well separated, LiVO_2 is a good compound in which to study magnetic frustration in a two-dimensional triangular lattice.

Stoichiometric LiVO_2 single crystals have never been successfully synthesized. The stoichiometry of LiVO_2 sample is best characterized by thermal cycling experiments. Previous studies by Goodenough et al. [15] on powders indicated that stoichiometric LiVO_2 is reversible on thermal cycling through T_t . On the other hand if the sample has lithium deficiency, heating $\text{Li}_{1-x}\text{VO}_2$ ($0.12 \leq x \leq 0.33$) through the phase transition temperature will result in the following irreversible disproportionation reaction:



Due to this reaction, LiV_2O_4 spinel phase formation will be observed for a non-stoichiometric sample when heating the sample through the transition temperature.

Although several studies have been carried out to elucidate the mechanism of the unusual phase transition in LiVO_2 , most of them were made on polycrystalline specimens. A few experiments were performed on non-stoichiometric single crystals [8,13,14]. Experimental results from previous studies are inconsistent, and the origin of the unusual magnetic transition and the ground state of this system still remain unclear. To explain the nature of the magnetic properties of this system, and clarify the trimer formation of vanadium ions in the crystal structure, systematic studies on stoichiometric LiVO_2 single crystals are required. In this study, we present a new technique of synthesizing large, high quality LiVO_2 single crystals and report basic characterization of the crystals by electron diffraction, magnetic susceptibility, electrical resistivity, differential scanning calorimetry, and specific heat experiments over an extended temperature range.

2. Crystal growth

The LiVO_2 single crystals in this study were grown by a LiBO_2 – Li_2O flux method similar to that reported in [13] except that in our method the growth occurs in sealed silica tubes instead of under flowing gas. LiVO_2 powder was prepared by direct solid state reaction of Li_2CO_3 (99.99%) and V_2O_3 (Johnson Matthey). The starting materials Li_2CO_3 and V_2O_3 were thoroughly ground together with a molar ratio of $\text{Li}/\text{V} = 1.01$ (1% lithium excess) and heated at 625°C for 24 h under flowing $\text{Ar}:\text{H}_2 = 96:4$ (%). The samples were furnace-cooled to room temperature and re-heated to 750°C for another 12 h after regrinding. The X-ray powder diffraction pattern of the obtained polycrystalline LiVO_2 sample indicates that the material is phase pure. To grow single crystals by a flux method, a mixture of 1.798 g LiVO_2 powder obtained above, 0.369 g Li_2O (99.5%) and 6.144 g LiBO_2 (99.997%) was placed in a platinum crucible and sealed in a quartz tube to prevent lithium volatilization. The crucible was maintained at 1100°C for 12 h and slowly cooled down to 700°C at a rate of $2\text{--}4^\circ\text{C}/\text{h}$, and then furnace-cooled to room temperature. The obtained single crystals were black, hexagonal platelets with typical size of $10\text{ mm} \times 10\text{ mm} \times 0.1\text{ mm}$ as shown in Fig. 2. Laue and 4-circle X-ray diffraction experiments show that they are single crystals and the hexagonal *ab*-plane is parallel to the flat faces of the crystals. Chemical analysis by inductively coupled plasma spectrometry gives the ratio of $\text{Li}/\text{V} = 0.98$, which indicates that crystals are nearly stoichiometric.



Fig. 2. Single crystals of LiVO_2 grown by the flux method described in the text.

3. Results and discussion

3.1. Electron diffraction

LiVO_2 single crystals were examined by transmission electron microscopy (TEM). TEM specimens were prepared by mechanically polishing the crystals to $\sim 10\ \mu\text{m}$ and then ion milling to electron transparency. As can be seen in Fig. 3 (and several other sample images), the crystals develop a network of microcracks that most likely form upon cooling through the first-order transition at 500 K. In many images the crack network appears to be hexagonal. The platelets are typically $0.3\text{--}0.8\ \mu\text{m}$ in diameter.

To perform electron diffraction experiments, the specimens were heated using a double-tilt heating stage in order to study the structural changes that occur at the transition temperature. This was complicated by the specimen crack networks that tended to thermally isolate each small platelet and by the relatively large lattice expansion that occurs at the transition temperature. At room temperature, the $\langle 0\ 0\ 1 \rangle$ zone axis diffraction pattern reveals superlattice reflections at $\{1/3\ 1/3\ 0\}$ consistent with the V^{3+} trimer model of Goodenough [7] (see Fig. 4a). Upon heating above 500 K, the specimen was observed to move (laterally and tilt) a relatively large amount. This made it impossible to measure the superlattice spot intensity as a function of temperature near the transition temperature. Above 530 K the movement was much diminished and in most areas of the specimen the superlattice reflections in the $\langle 0\ 0\ 1 \rangle$ zone axis diffraction pattern had disappeared (see Fig. 4b). Upon cooling to below 500 K, the large movements return (before the superlattice reflections appear). Below 470 K, the superlattice spots reappear (see Fig. 4c). The maximum specimen displacements were found to occur at an indicated temperature of $\sim 520\ \text{K}$ on heating and $\sim 490\ \text{K}$ on cooling.

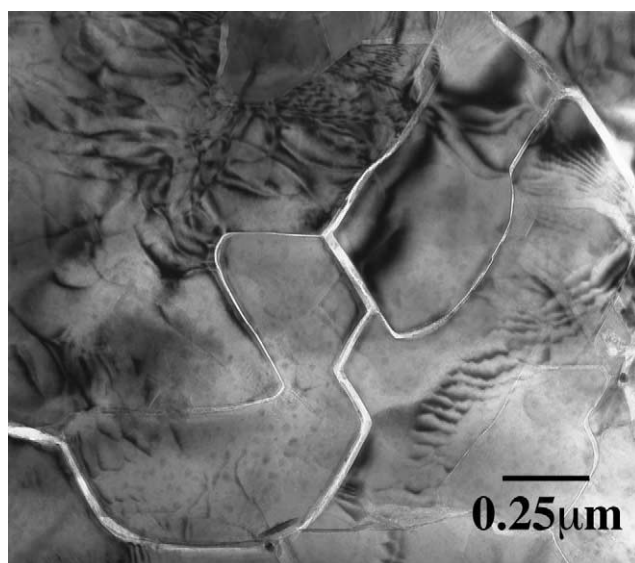


Fig. 3. Representative bright field electron micrograph of a LiVO_2 crystal showing the network of microcracks that develops in the crystals.

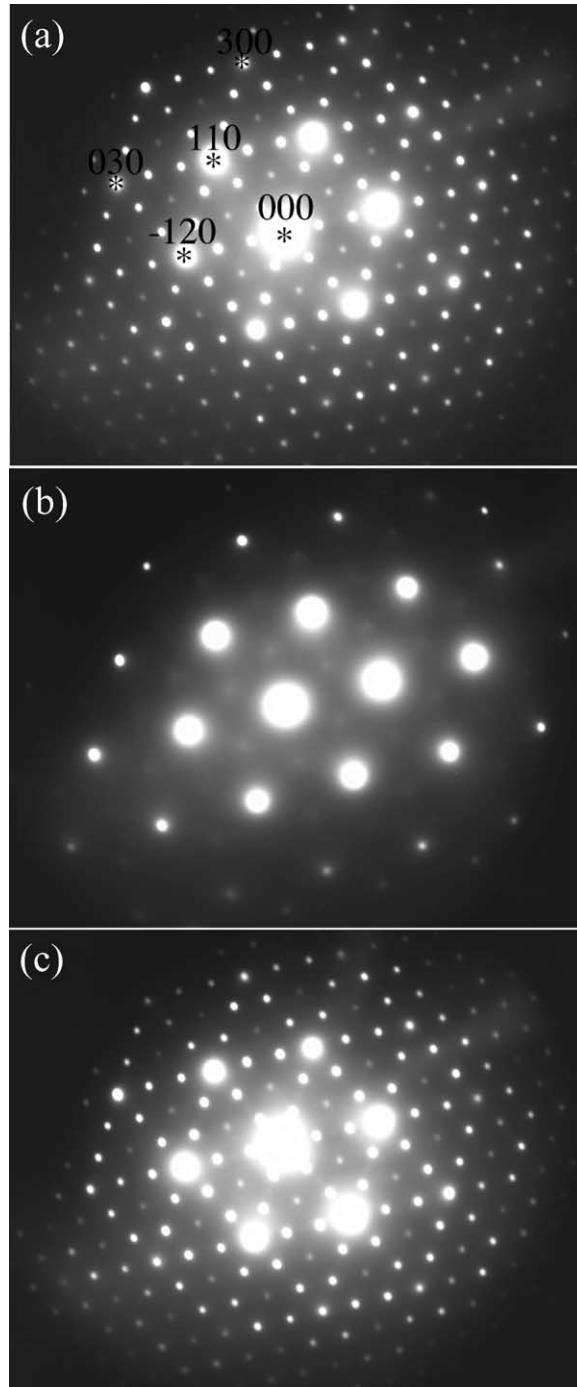


Fig. 4. Electron diffraction patterns from the $\langle 001 \rangle$ zone axis of a LiVO_2 single crystal. (a) Pattern at room temperature with $\{1/3\ 1/3\ 0\}$ -type superlattice reflections. (b) Pattern after heating to 530 K shows the disappearance of the superlattice spots above the transition temperature. (c) Pattern after cooling to 470 K. The superlattice spots have reappeared.

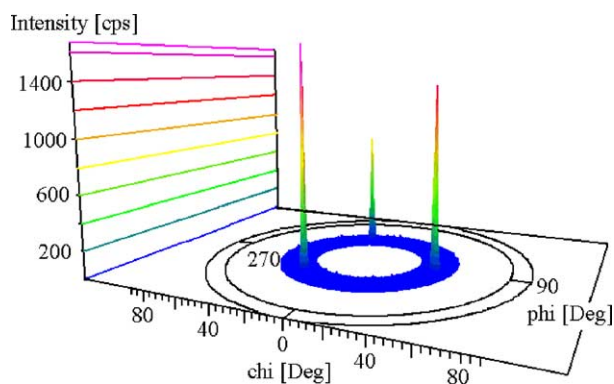


Fig. 5. Pole figure of LiVO_2 (1 0 7) reflection.

3.2. 4-Circle X-ray diffraction

To verify the quality of the LiVO_2 single crystals, 4-circle X-ray diffraction experiments were performed on a Scintag PTS 4-circle machine. Fig. 5 shows a representative scan of a LiVO_2 (107) reflection. As is clear from the figure, a three-fold symmetry was observed and the width of the peaks is about 3° . It indicates that despite the microcracking, the samples are still monocrystalline in the sense that long range translational order is preserved.

3.3. Magnetic susceptibility

Measurement of the magnetic susceptibility from 2 to 300 K was performed using a SQUID magnetometer in an applied field of 1 kOe. The susceptibility above room temperature was measured using a Faraday balance magnetometer with an applied field of 7 kOe.

Fig. 6 shows the temperature dependence of the dc magnetic susceptibility of a LiVO_2 sample consisting of a large number of randomly oriented small single crystals from the flux growths. As shown in the inset of Fig. 6, a first-order phase transition occurs at $T_c \approx 500$ K on heating and $T_c \approx 440$ K on cooling. These results are consistent with a previous study performed on a stoichiometric LiVO_2 powder sample [16]. Above the transition temperature, it appears that χ decreases slightly with increasing temperature and roughly follows the Curie–Weiss law $\chi = C/(T - \theta)$, where C is the Curie constant and θ is the Curie–Weiss temperature. By fitting the data between 440 and 650 K with a Curie–Weiss law, we obtained $\theta = -1549$ K and $\mu_{\text{eff}} = 3.35\mu_B$. These values have a large uncertainty due to the narrow fitting range. The effective moment is close to $2.83\mu_B$ (the effective moment of a V^{3+} ion with $g = 2$ and $S = 1$) which indicates that the magnetic state of V ions above the transition temperature can be nearly explained by a local moment model with $S = 1$. Below the phase transition temperature, χ is nearly non-magnetic and increases gradually with decreasing temperature with an upturn at low temperature. Fitting the low-temperature data with a Curie–Weiss law, the obtained effective moment is $0.39\mu_B$. If we attribute the Curie–Weiss tail to the excess V^{4+} ions due to nonstoichiometry of the sample, we may infer from the obtained effective moment that the Li deficiency in this sample is about 5%, which is in reasonable accord with the ICP result of 2% Li deficiency.

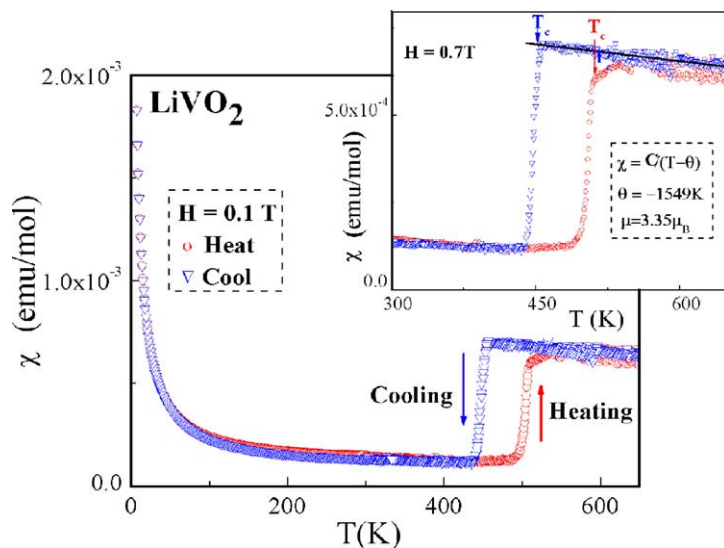


Fig. 6. Temperature dependence of the dc magnetic susceptibility of LiVO_2 . The solid line in the inset is the Curie–Weiss fit.

3.4. Differential scanning calorimetry and specific heat

The thermodynamic properties of LiVO_2 were investigated by differential scanning calorimetry (DSC) and specific heat measurements. The DSC experiments were performed using a Perkin-Elmer thermal analysis control system 7/4, while the specific heat was measured using a commercial heat pulse calorimeter from Quantum Design.

Fig. 7 shows the DSC traces obtained using a heating and cooling rate of $10^\circ\text{C}/\text{min}$ between 400 and 520 K; it reconfirmed the first order phase transition at about 490 K on heating and at about 440 K on cooling, which agrees very well with the susceptibility measurements. The calculated enthalpy change is about 3.6 kcal/mol.

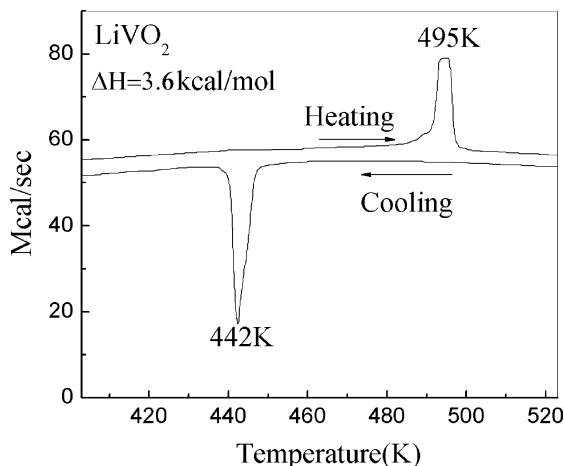


Fig. 7. Phase transition observed by DSC.

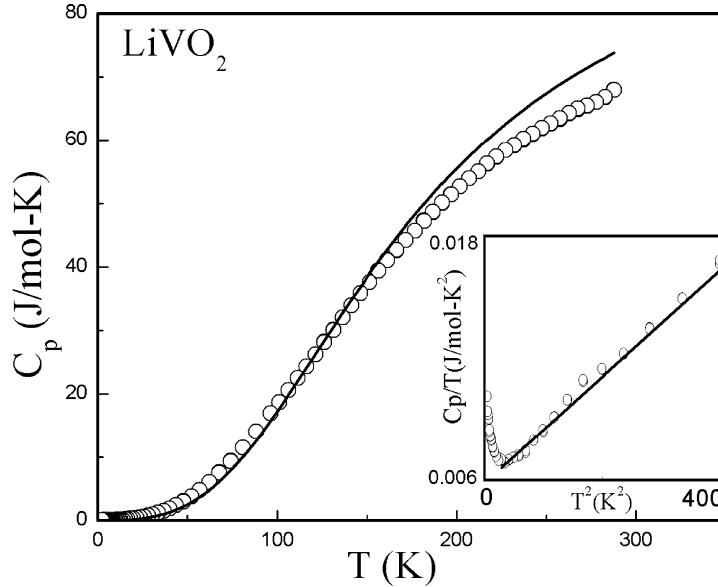


Fig. 8. Temperature dependence of the specific heat (open circles). Solid line is the best fit using Eq. (1). The inset is the specific heat data between 2 and 20 K plotted as C_p/T vs. T^2 . The solid line in the inset is the fit to $C_p/T = \gamma + \beta T^2$ (5–20 K) from which a Debye temperature of $\theta_D = 657$ K can be inferred.

The temperature dependence of the specific heat from 2 to 295 K is shown in Fig. 8. No anomaly is apparent, and the specific heat has not approached its Dulong and Petit value of 99.8 J/mol/K which indicates a Debye temperature substantially greater than room temperature. The small upturn observed below 5 K may be due to a Schottky anomaly, although we have not attempted any detailed modeling.

According to the Debye model, the specific heat of a crystal is given by:

$$C_v = 9nk_B \left(\frac{T}{\theta_D} \right)^3 \int_0^{\theta_D/T} \frac{x^4 e^x dx}{(e^x - 1)^2}, \quad (1)$$

where n is number of ions per unit volume in the crystal, k_B is Boltzmann's constant, and θ_D is Debye temperature. Using Eq. (1) to model the specific heat, we find the best fit over the whole data range is given by choosing $\theta_D = 730$ K, although as is clear from the Figure the Debye model does not do a particularly good job of describing the specific heat over the entire temperature range. Another way of estimating the Debye temperature is to fit low-temperature specific data to $C_p/T = \gamma + \beta T^2$. Using this approach to fit the data between 5 and 20 K (see Fig. 8 inset) yields $\gamma = 5.8$ mJ/mol/K² and $\beta = 0.027$ mJ/mol/K⁴; the calculated Debye temperature obtained from β is $\theta_D = 657$ K.

3.5. Resistivity

Using a conventional four-probe technique, the *ab*-plane and *c*-axis resistivities of LiVO₂ single crystals were investigated from 40 to 600 K. The first-order phase transition was observed in *ab*-plane and *c*-axis resistivities as shown in Fig. 9a. The transition temperature agrees with the susceptibility and DSC results. As we can see in Fig. 9a, both *ab*-plane and *c*-axis resistivities increase very rapidly with

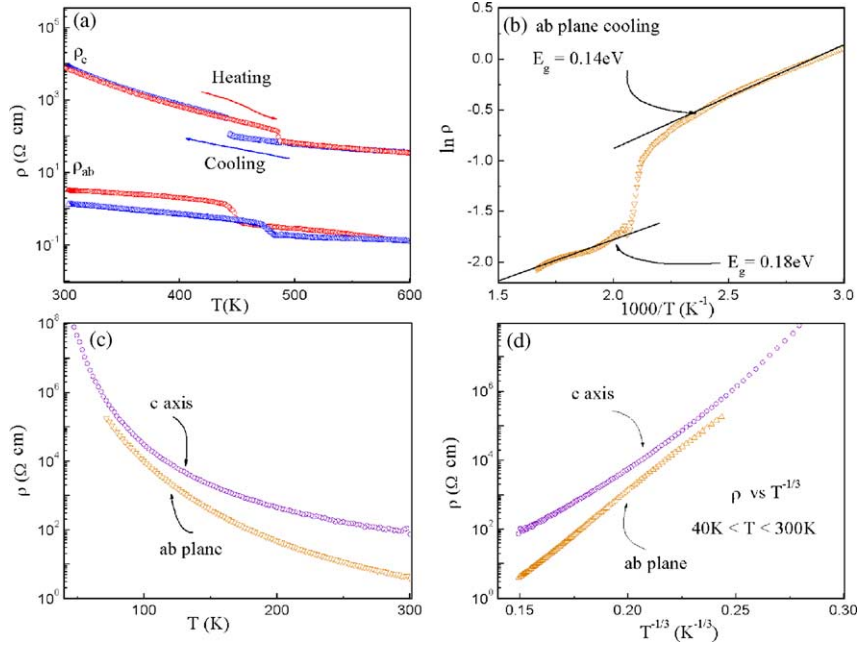


Fig. 9. (a) Temperature dependence of the *ab*-plane and *c*-axis resistivities of LiVO_2 between 300 and 600 K. (b) Energy gaps inferred from Arrhenius fits. (c) Temperature dependence of the *ab*-plane and *c*-axis resistivities of LiVO_2 between 40 and 300 K. (d) ρ_{ab} and ρ_c vs. $T^{-1/3}$ between 40 and 300 K.

decreasing temperature. LiVO_2 shows semiconducting behavior below and above the transition temperature. For a semiconductor we expect:

$$\rho \propto e^{-E_g/2k_B T}, \quad (2)$$

where E_g is the semiconducting energy gap and k_B is Boltzmann's constant. In Fig. 9b, we plot $\ln(\rho)$ versus T^{-1} and find that the behavior is roughly linear below and above the transition temperature. This suggests that the system can be treated as a semiconductor. Although we expect that the measured value of the resistivity is larger than the intrinsic value due to microcracking, the microcracking should not affect the Arrhenius behavior of the system. The solid lines in the Fig. 9b are fits to Eq. (2) both below and above the transition temperature; the obtained E_g is about 0.18 eV for $T > T_t$ and 0.14 eV for $T < T_t$ and agrees with the results reported in [13]. Fig. 9c shows the temperature dependence of the *ab*-plane and *c*-axis resistivities between 40 and 300 K. Both Fig. 9a and c show that the ratio of ρ_c/ρ_{ab} is about 100. Fig. 9d is a plot of the *ab*-plane and *c*-axis resistivity on a log scale versus $T^{-1/3}$ between 40 and 300 K. The plot indicates that the in-plane low-temperature resistivity of LiVO_2 appears to obey the Mott $T^{-1/3}$ law, suggesting 2D variable range hopping in the low-temperature regime.

4. Conclusion

In summary, an improved synthesis technique for growing LiVO_2 single crystals is reported. The obtained crystals were studied by $\chi(T)$, $\rho(T)$, $C_p(T)$, and DSC measurements from 2 to 650 K.

A first-order phase transition was observed in all experiments with a consistent transition temperature 500 K upon heating. The inferred (high temperature) Weiss and Debye temperatures are about –1549 K and 657 K, respectively. The system shows semiconducting behavior with resistivity anisotropy of roughly 100. Electron diffraction experiments on LiVO_2 single crystals show that the superlattice reflections do indeed disappear above the phase transition temperature consistent with Goodenough's "trimer" model. Neutron scattering experiments will be carried out on the LiVO_2 single crystals to study the magnetic behavior of this system.

Acknowledgements

The author would like to thank Dr. J.L. Musfeldt, T. Barnes, and N.J. Dudney for helpful discussions. Oak Ridge National laboratory is managed by UT-Battelle, LLC, for the US Department of Energy under contract DE-AC05-00OR22725.

References

- [1] K. Mizushima, P.C. Jones, P.J. Wiseman, J.B. Goodenough, *Mater. Res. Bull.* 15 (1980) 783.
- [2] C. Plichta, M. Salomon, S. Slane, M. Uchiyoma, B. Chua, W.B. Ebner, H.W. Lin, *J. Power Source* 21 (1987) 25.
- [3] L.A. de Picciotto, M.M. Thackeray, G. Pistoia, *Solid State Ionics* 28–30 (1988) 1364.
- [4] J.B. Goodenough, A. Manthiram, W.P. James, *Mater. Res. Soc. Symp.* 135 (1989) 391.
- [5] P.F. Bongers, Ph.D. Thesis, University of Leiden, Leiden, The Netherlands, 1957.
- [6] B. Rutter, R. Weber, J. Jaskowski, *Z. Elektrochem.* 66 (1962) 832.
- [7] J.B. Goodenough, *Phys. Rev.* 120 (1960) 67.
- [8] T.A. Hewston, B.L. Chamberland, *J. Solid State Chem.* 59 (1985) 168.
- [9] A. Manthiram, J.B. Goodenough, *Can. J. Phys.* 65 (1987) 309.
- [10] J.B. Goodenough, *Magnetism and the Chemical Bond*, Interscience, New York, 1963.
- [11] K. Kobayashi, K. Kosuge, S. Kachi, *Mater. Res. Bull.* 4 (1969) 95.
- [12] H.F. Pen, van den Brink, D.I. Khomskii, G.A. Sawatzky, *Phys. Rev. Lett.* 78 (1997) 1323.
- [13] H. Takei, M. Koike, K. Imai, H. Sawa, H. Kadowaki, Y. Iye, *Mater. Res. Bull.* 27 (1992) 555.
- [14] K. Imai, H. Sawa, M. Koike, M. Hasegawa, H. Takei, *J. Solid State Chem.* 114 (1995) 184.
- [15] J.B. Goodenough, G. Dutta, A. Manthiram, *Phys. Rev. B* 43 (1991) 10170.
- [16] M. Onoda, T. Naka, H. Nagasawa, *J. Phys. Soc. Jpn.* 60 (1991) 2550.